Thermionic trap-assisted tunneling model and its application to leakage current in nitrided oxides and Al Ga N Ga N high electron mobility transistors

D. Mahaveer Sathaiya and Shreepad Karmalkar

Citation: Journal of Applied Physics **99**, 093701 (2006); doi: 10.1063/1.2191620
View online: http://dx.doi.org/10.1063/1.2191620
View Table of Contents: http://scitation.aip.org/content/aip/journal/jap/99/9?ver=pdfcov
Published by the AIP Publishing

Thermionic trap-assisted tunneling model and its application to leakage current in nitrided oxides and AlGaN/GaN high electron mobility transistors

D. Mahaveer Sathaiya[a] and Shreepad Karmalkar
Department of Electrical Engineering, Indian Institute of Technology, Madras 600 036, India

(Received 5 January 2006; accepted 8 March 2006; published online 11 May 2006)

We propose two models of electron tunneling from metal to a semiconductor via traps. In addition to the electrons below the metal Fermi level, the models also include the thermally activated electrons above the Fermi level. The first model is called generalized thermionic trap-assisted tunneling (GTTT), which considers tunneling through both triangular and trapezoidal barriers present in metal insulator semiconductor (MIS) structures. The second model is called thermionic trap-assisted tunneling (TTT), which considers tunneling through triangular barriers present in modern Schottky junctions. The GTTT model is shown to predict the low field leakage currents in MIS structures with nitrided oxide as insulator, and the TTT model is shown to predict the reverse gate leakage in AlGaN/GaN high electron mobility transistors. © *2006 American Institute of Physics*. [DOI: 10.1063/1.2191620]

I. INTRODUCTION

Trap-assisted tunneling is widely regarded to be the mechanism of the leakage current through nitrided and tunnel oxides[1] and the stress-induced leakage current (SILC).[2] Using this mechanism, Suzuki and Schroder[3] explained the enhanced conduction through nitrided oxide at low fields (<4 MV/cm). Later Cheng *et al.*[1] showed that the current through nitrided oxide increases with nitridation due to an increase in electron trap concentration. An analytical model for trap-assisted tunneling through a triangular barrier which occurs at high field was proposed by Fleisicher and Lai.[4] Houng *et al.*[5] showed that trap-assisted tunneling at low fields occurs through a trapezoidal barrier [see Fig. 1(a)] and proposed a generalized model including both trapezoidal and triangular barrier tunneling components. In our previous work,[6] we used a trap-assisted tunneling model involving a band of traps to explain the large reverse leakage[7] of the Schottky-type gate junction of AlGaN/GaN high electron mobility transistors (HEMTs).

In the present article, GTT denotes the existing model of generalized trap-assisted tunneling through both triangular and trapezoidal barriers [see Fig. 1(a)] present in metal insulator semiconductor (MIS) structures. On the other hand, TT denotes the existing model of trap-assisted tunneling only through a triangular barrier [see Fig. 1(b)] seen in modern Schottky junctions such as gate junction of AlGaN/GaN HEMTs.[6,8]

Refer to the GTT and TT models shown in Figs. 1(a) and 1(b). Here the electron tunneling is assumed to take place below the metal Fermi level, irrespective of the location of the trap level (ϕ_t) with respect to this Fermi level. In Fig. 1 the metal Fermi level is located at the point $\phi=\phi_B$, where ϕ_B denotes the barrier height. Possible electron tunneling above the Fermi level for $\phi_t<\phi_B$ due to thermal activation, shown in Figs. 1(c) and 1(d), has been neglected in these models. As we show in this paper, the tunneling current including thermal activation is several orders of magnitude higher than that given by the GTT and TT models, at low electric fields.

In this paper, we propose trap-assisted tunneling models, which include thermally activated electrons, and discuss their applications. These models are called generalized thermionic trap-assisted tunneling (GTTT) [see Fig. 1(c)] and thermionic trap-assisted tunneling (TTT) [see Fig. 1(d)]. Here, the word "thermionic" denotes the thermally activated electrons. First we present the GTTT model and its application to leakage current in MIS structures with nitrided oxide

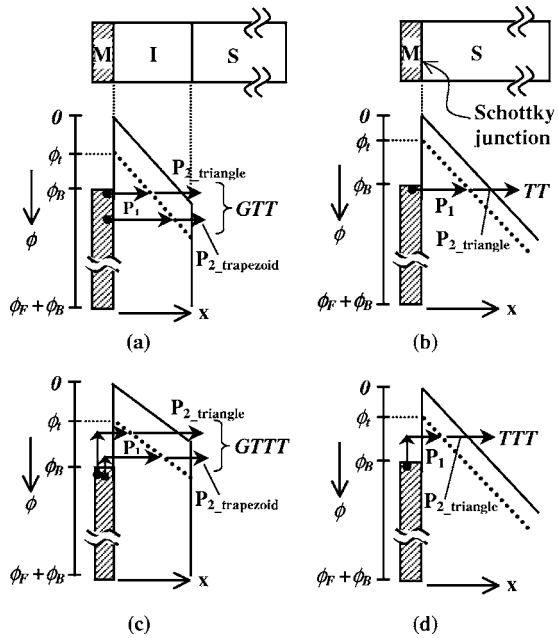

FIG. 1. Device structure and energy band diagrams of reverse biased MIS structure and Schottky diode. The existing GTT (a) and TT (b) models and the proposed GTTT (c) and TTT (d) models are shown. ϕ_t is the trap ionization energy and ϕ_B is the barrier height.

[a]FAX: 91-44-2257-4402; electronic mail: sathaiya@yahoo.co.in

as insulator. Then we present the TTT model and its applications to the gate leakage current in AlGaN/GaN HEMTs.

II. GENERALIZED THERMIONIC TRAP-ASSISTED TUNNELING (GTTT)

Our GTTT model, shown in Fig. 1(c), incorporates the thermally activated electrons by including the Fermi-Dirac function ignored in the GTT model of Houng *et al.*[5] Additional differences between the GTT and GTTT models will be discussed shortly. The equation for our GTTT model is given by

$$J_{\mathrm{GTTT}} = \frac{qC_tN_t}{E}\left[\int_{\phi_t}^{\phi_t+Ed}\left(\frac{1}{f_{\mathrm{FD}}P_1}+\frac{1}{P_{2\_\mathrm{trapezoid}}}\right)^{-1}d\phi\right] \quad \text{for } E \leqslant \frac{\phi_t}{d}, \tag{1}$$

$$J_{\mathrm{GTTT}} = \frac{qC_tN_t}{E}\left[\int_{\phi_t}^{Ed}\left(\frac{1}{f_{\mathrm{FD}}P_1}+\frac{1}{P_{2\_\mathrm{triangle}}}\right)^{-1}d\phi + \int_{Ed}^{\phi_t+Ed}\left(\frac{1}{f_{\mathrm{FD}}P_1}+\frac{1}{P_{2\_\mathrm{trapezoid}}}\right)^{-1}d\phi\right] \quad \text{for } E > \frac{\phi_t}{d}, \tag{2}$$

where E is the electric field across the insulator, d is the insulator thickness, N_t is the uniform trap concentration, f_{FD} is the Fermi-Dirac function given by

$$f_{\mathrm{FD}} = \frac{1}{1+\exp[q(\phi_B-\phi)/kT]}, \tag{3}$$

P_1, P_{2_triangle}, and $P_{2\_\mathrm{trapezoid}}$ are the tunneling probabilities based on WKB approximations for the two-step process [see Fig. 1(c)],

$$P_1 = \exp\left[-\frac{\alpha}{E}(\phi^{3/2}-\phi_t^{3/2})\right], \quad P_{2\_\mathrm{triangle}} = \exp\left(-\frac{\alpha}{E}\phi_t^{3/2}\right),$$

$$P_{2\_\mathrm{trapezoid}} = \exp\left\{-\frac{\alpha}{E}[\phi_t^{3/2}-(\phi-Ed)^{3/2}]\right\}, \quad \alpha = \frac{8\pi\sqrt{2m_Iq}}{3h}, \tag{4}$$

and C_t is the trap energy dependent rate constant[4] given by

$$C_t = \left(\frac{m_M}{m_I}\right)^{5/2}\frac{16\pi q\phi_1^{3/2}}{3h\sqrt{\phi_t-\phi_1}}, \quad \phi_1 = 0.2\ \mathrm{V}. \tag{5}$$

Apart from the presence of the Fermi-Dirac function, Eqs. (1) and (2) differ from the equation of Houng *et al.* in the following respects. The GTT model[5] integrates the current equation with respect to distance (x) and does not explain the integration limits for triangular and trapezoidal barrier tunnelings. In contrast, our model integrates with respect to the energy (ϕ) [see Eqs. (1) and (2)] and thus allows easy visualization of the integration limits directly from the energy band diagram. The limits in Eqs. (1) and (2) can be understood from the band diagrams shown in Figs. 2(a) and 2(b), respectively.

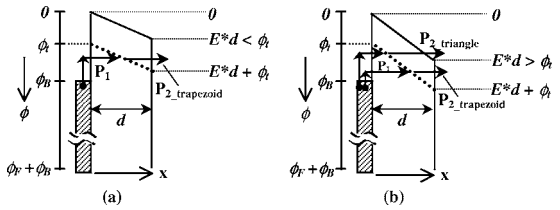

FIG. 2. Energy band diagram of a reverse biased MIS structure for $Ed < \phi_t$ (a) corresponding to Eq. (1) and for $Ed > \phi_t$ (b) corresponding to Eq. (2).

In Fig. 3, we show the calculations of the total tunneling current togther with its triangular and trapezoidal components, for a typical metal-nitrided oxide-semiconductor structure over the electric field range of 0–5 MV/cm. It is seen that the total current flows through the trapezoidal barrier at low fields $E \leqslant (\phi_t/d)$ and through the triangular barrier at high fields $E \geqslant (\phi_t/d)$. The triangular component is zero for $E < (\phi_t/d)$, because traps are not present in the triangular barrier region for this condition, as seen from the energy band diagram of Fig. 2(a). Also, it is seen that the GTTT current at 400 K is more than that at 300 K due to the increase in thermally activated electron tunneling with temperature.

Calculations of the GTTT and GTT currents through the above MIS structure are shown in Fig. 4. It is seen that the GTTT current is several orders of magnitude higher than GTT current at low fields [see Fig. 4(a)]. But at high fields, the difference between GTTT and GTT currents is small [see Fig. 4(b)]. This is because, as the field increases, the tunneling barrier for electrons at the Fermi level becomes thinner. Consequently, electron tunneling at the Fermi level starts dominating the thermally activated electron tunneling. This is also the reason why the difference between the 300 and 400 K GTTT currents at high fields in Fig. 3 is small. It is mentioned here that we calculated the GTT current using a modified version of the GTT model[5] of Houng *et al.* given in detail in Appendix. This version developed by us is clear about the integration limits associated with the triangular and trapezoidal components. It also shows that, when $\phi_t < \phi_B$,

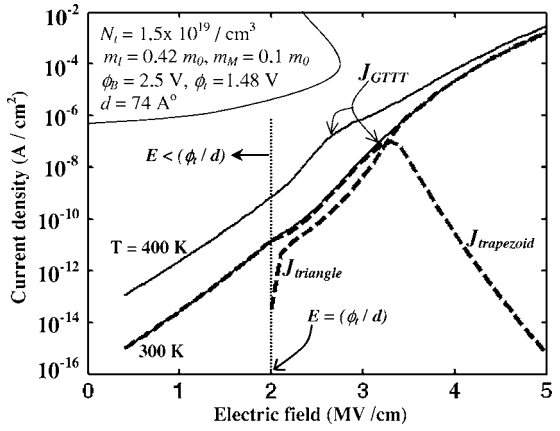

FIG. 3. Total tunneling current (J_{GTTT}) togther with its triangular (J_{triangle}) and trapezoidal ($J_{\mathrm{trapezoid}}$) components over the electric field range of 0–5 MV/cm. Only the total current (J_{GTTT}) is shown for T=400 K. Here calculations are based on the parameter values given in the inset. N_t is the trap concentration, m is the effective mass, and d is the insulator thickness.

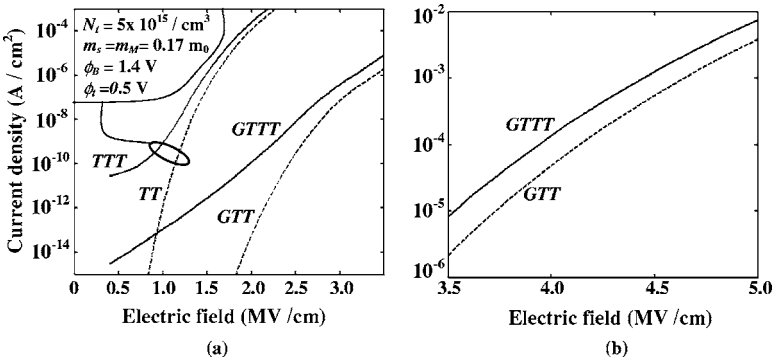

FIG. 4. GTTT current (solid line) at temperature $T=300$ K and GTT current (dashed line) for low electric field range (a) and high electric field range (b). Parameter values used for GTTT and GTT are given in the inset in Fig. 3; $\phi_t=1.6$ V. These values correspond to nitrided oxide (see Ref. 5). Also shown are the TTT current (solid line) at $T=300$ K and TT current (dashed line) in (a). Parameter values used for TTT and TT are given in the inset in (a). These values correspond to AlGaN/GaN HEMT (see Ref. 6).

the GTT is zero for fields below $E_{\min}$ (see Appendix), because the GTT model does not consider tunneling above metal Fermi level. Note that such an issue does not arise in the GTTT model. In the GTTT model given above, a single set of equations covers both the cases $\phi_t < \phi_B$ and $\phi_t > \phi_B$. In contrast, the equations for these two cases are different in the GTT model (see Appendix). Hence, the ϕ_t extraction from the experimental data using the GTTT model will be easier than using the GTT model.

Next we compare our model with the measured current through nitrided oxide in the low field range of 1–4 MV/cm reported in Ref. 3. In model calculations, we incorporate the image force and quantum barrier lowering, given by the following relation:[9]

$$\phi_B = \phi_{B0} - \alpha E^{1/2} - \beta E^{2/3}. \tag{6}$$

Here α and β are the image force and quantum barrier lowering parameters, respectively. The calculations are performed numerically. We have split the model parameters into two categories, primary and secondary. Primary parameters, ϕ_{B0}, ϕ_t, and N_t, are extracted from the best GTTT model fit to measured data. Secondary parameters, α, β, and the effective mass m, are assumed based on material properties. All the parameter values are given in Fig. 5. The GTTT model fits into the experimental data. The GTT current calculated using the same parameter values and equations in Appendix is also shown. This current does not match the experimental data below 1.75 MV/cm and is lower by more than two orders of magnitude. For fields higher than 1.75 MV/cm, the GTT current matches with the GTTT current because tunneling below the metal Fermi level dominates over the thermally activated current. The field beyond which GTT matches with GTTT increases with decreasing ϕ_t.

Note that Houng *et al.*[5] have employed parameter values of $\phi_t=2.83$ V, $\phi_B=2.5$ V, and $N_t=8\times10^{14}$/cm^3 for fitting the same measured data. These values are different from those employed by us. We have found that if these parameters are used in the GTT equations given by us in Appendix, the GTT current is ten orders of magnitude lower than the measured data. Efforts to raise this current by increasing N_t by ten orders of magnitude result in a curve which passes through only one of the measured points, because the shape of the model curve differs significantly from that of the measured data. The shape of the GTT current depends mainly on the relative values of ϕ_t and ϕ_B and not on N_t. Finally, the value of ϕ_B used by Houng *et al.*[5] is an effective barrier height, neglecting barrier lowering effects.

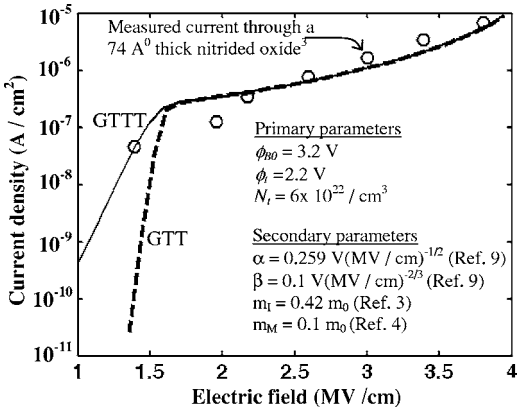

FIG. 5. GTTT model fit (solid line) to experimental data (points) from Ref. 3 using the parameter values given in the inset. Also shown are the GTT model results (dashed line) for the same parameter values.

III. THERMIONIC TRAP-ASSISTED TUNNELING (TTT)

Our TTT model [see Fig. 1(d)] incorporates the thermally activated electrons by including the Fermi-Dirac function ignored in the TT model of Cheng *et al.*[1] The mathematical representation of our TTT model is

$$J_{\mathrm{TTT}} = \frac{qC_tN_t}{E}\int_{\phi_t}^{\phi_B+\phi_F}\left(\frac{1}{f_{\mathrm{FD}}P_1}+\frac{1}{P_{2\_\mathrm{triangle}}}\right)^{-1}d\phi. \tag{7}$$

Here E is the electric field at the Schottky junction and the other symbols have the same meaning as in the GTTT model [Eqs. (1)–(5)] except the effective mass in insulator (m_I) which is replaced by effective mass in semiconductor (m_s). Inclusion of the Fermi-Dirac function in TTT model makes analytical integration in Eq. (7) difficult. So, in this paper, TTT model results are obtained numerically.

To show the applicability of the TTT model, we consider the large reverse leakage[7,10] observed in the Schottky-type gate junction of AlGaN/GaN HEMTs. This current can be as much as two orders of magnitude more than that in AlGaAs/GaAs HEMTs.[7] To reduce this current and thus suppress noise and power consumption, it is important to understand its mechanism. In our recent work,[11] we showed that direct tunneling mechanisms such as thermionic field emission (TFE), FE, or tunneling through a thin surface barrier[12] are unlikely causes of this current, because their high sensi-

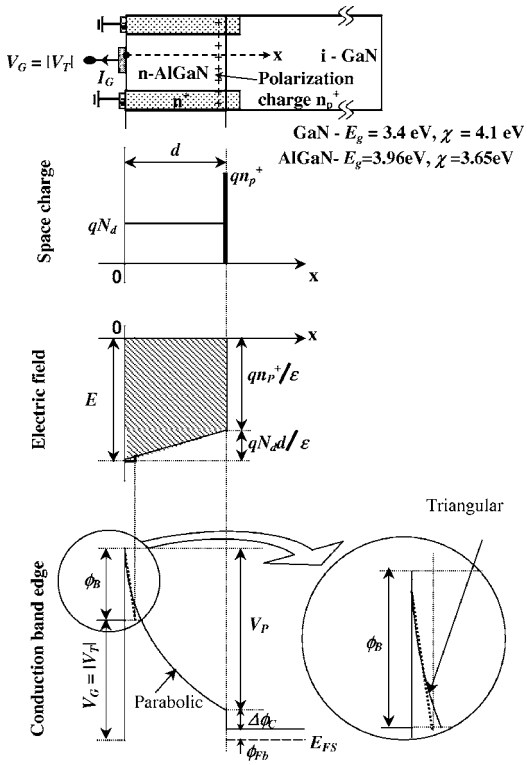

FIG. 6. Space charge, electric field, and conduction band diagram along a horizontal line passing through the center of gate length in AlGaN/GaN HEMT structure. The device is biased at $V_G=|V_T|$, which is the threshold voltage. The triangular approximation for a fraction of the parabolic barrier through which the electron tunneling occurs is also shown.

tivity to electric field is in disagreement with the low sensitivity shown by the measured data. As we show below, our TTT model can explain this current.

The gate current can be written as

$$I_G = SJ_{\mathrm{TTT}}, \tag{8}$$

where S denotes the gate area and J_{TTT} is given in Eq. (7). The assumption of a triangular approximation for the gate potential barrier is justified, since the percentage change in the electric field over the barrier thickness through which tunneling occurs is small due to the polarization sheet charge at the heterojunction (see Fig. 6). Thus, the electric field in the small portion of the AlGaN layer through which tunneling occurs is assumed to be constant and equal to the peak electric field at the gate junction, given by

$$E = \frac{V_P + qN_d d^2/2\varepsilon}{d} \quad \text{for } V_G \leqslant |V_T|,$$
$$V_P = V_G + \phi_B - \Delta\phi_C - \phi_{fb}. \tag{9}$$

V_p, ϕ_B, $\Delta\phi_C$, d, and ϕ_{fb} are shown in Fig. 6. The magnitude of I_G saturates for $V_G \geqslant |V_T|$,[8] where V_G is the reverse voltage magnitude and V_T is the device threshold voltage. This is because the vertical electric field picture beneath the gate, which controls I_G, does not change for $V_G > |V_T|$, and the extra voltage $V_G - |V_T|$ drops laterally from gate to drain/source. Note that the higher the $|V_T|$, the higher is the value at which I_G saturates.

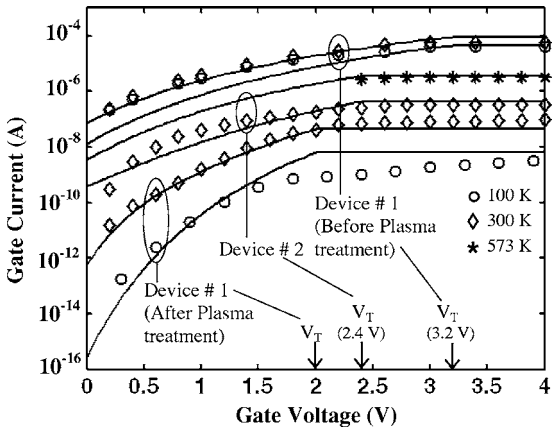

FIG. 7. TTT model fit (solid lines) to experimental data (points) using the parameters given in the Table I, and $m_s=0.17m_0$, $\gamma_1=0.4$, and $\gamma_T=2.7\times10^{-4}$ V/K. For device 1, $d=200$ Å and $S=1.1\times100$ μm^2 (see Ref. 7), and for device 2, $d=250$ Å and $S=1\times100$ μm^2 (see Ref. 10). For device 2 at 573 K only saturation data are available in Ref. 10.

It is necessary to incorporate image force barrier lowering[13] and band gap reduction with temperature[14,15] while calculating I_G [these effects are, however, not to be included in the V_p formula Eq. (9)]. These effects are given by the following relation:[6]

$$\phi_B = \phi_{B0} - \gamma_I \sqrt{\frac{q}{\pi\varepsilon}}\sqrt{E} - \gamma_T T. \tag{10}$$

In this I_G calculation, ϕ_{B0}, ϕ_t, N_t, and N_d are the primary parameters extracted from the best model fit to experimental data, and V_p, γ_I, γ_T, ε (AlGaN), and effective mass m are the secondary parameters assumed based on material properties. The assumed values are $m_s=0.17m_0$,[6] (average of $0.1m_0$ in metal[4] and $0.23m_0$ in AlGaN),[16] ε (AlGaN)=8.9, $\gamma_1=0.4$ (Ref. 6), and $\gamma_T=2.7\times10^{-4}$ V/K.[16] V_p is calculated using $\Delta\phi_c=0.4$ V and $\phi_{fb}=0.2$ V [see Eq. (9)].

Consider the experimental I_G-V_G data of device 1 shown in Fig. 7. These data correspond to a HEMT before and after plasma treatment and is taken from Ref. 7. Important features of these data are as follows. Prior to the plasma treatment, $|V_T|=3.2$ V, and the current is high and almost insensitive to temperature between 100 and 300 K. After treatment, $|V_T|$ reduces to 2 V; the saturation I_G is suppressed but becomes sensitive to temperature, increasing by a factor of ~30 from 100 to 300 K. We could fit our model into these data as shown in Fig. 7. The parameters extracted from this fit are given in Table I. The trap location (ϕ_t) extracted

TABLE I. Extracted model parameters.

Parameter	Device 1[a]	Device 1[b]	Device 2
ϕ_{B0}(V)	1.44	1.44	1.5
ϕ_t(V)	0.85	0.78	0.79
N_t(cm^{-3})	2×10^{16}	5×10^{14}	3×10^{15}
N_D(cm^{-3})	4.8×10^{18}	1.9×10^{18}	3.1×10^{18}

[a]Before plasma treatment.
[b]After plasma treatment.

from the data prior to the plasma treatment is 0.85 V below the conduction band edge. Plasma treatment moves the trap location up to 0.78 V below the conduction band edge and suppresses N_t by a factor of ~40 and N_d by a factor of ~2.5. The reduction in N_d is solely responsible for the observed reduction in $|V_T|$ from 3.2 to 2 V due to plasma treatment. The reduction in $|V_T|$ and N_t is responsible for the decrease in I_G. The reduction in ϕ_t from 0.85 to 0.78 V causes the increased temperature dependence of I_G. Thus we conclude that the gate current at 100 and 300 K is dominated by TTT, independent of the processes such as plasma treatment used in device fabrication. To illustrate the importance of TTT at higher temperatures, we consider device 2 in Fig. 7, whose measured I_G rises by an order of magnitude from 300 to 573 K.[10] As can be seen, our model successfully predicts this reported I_G data also. The parameters used in this prediction appear in Table I. The extracted ϕ_{B0} of device 2 with d=250 Å is 0.06 V more than that of device 1 with d =200 Å. This is consistent with observations in Ref. 17 that ϕ_{B0} increases with AlGaN layer thickness (d). Further, ϕ_{B0} and N_d affect both TTT and direct tunneling (TFE and FE) which are present in parallel.[6] The values of these parameters are such that TTT current dominates over the direct tunneling current (which cannot fit the shape of the leakage current).

It is of interest to compare the present model with our earlier model[6] of the gate leakage current in AlGaN/GaN HEMTs. In that model,[6] two different mechanisms were required to explain the data of Fig. 7; while the current at 100 and 300 K was explained using trap-assisted tunneling through a band of traps, the current at 573 K was explained using direct tunneling (TFE). However, in the present paper, a single mechanism, namely, TTT, is used to explain the current behavior over the entire temperature range. Also, this mechanism based on a single trap level is much simpler than the trap-assisted tunneling based on a trap band.[6]

IV. CONCLUSION

We proposed two trap-assisted tunneling models, which take into account the extra electron tunneling above the metal Fermi level due to thermal activation. One model is called generalized thermionic trap-assisted tunneling (GTTT) which includes flow through both triangular and trapezoidal barriers. We showed how this model predicts the leakage current through MIS structures at low fields. Low field current measurements at higher temperature will provide further evidence of the presence of GTTT current. Another model is called thermionic trap-assisted tunneling (TTT), which occurs through only triangular barrier. We discussed the application of this model to the reverse gate leakage in AlGaN/GaN HEMTs. The proposed models are useful to predict the leakage currents in modern electronic devices.

APPENDIX

Here we present the equations for the GTT model proposed in Ref. 5, with a significant modification that the integration of the current equation is carried out with respect to energy ϕ rather than the distance x. This modification clearly reveals the integration limits associated with triangular and trapezoidal components. It also brings out a minimum field condition on the GTT current, which is not discussed in Ref. 5. We have used this modified GTT model for the GTT current calculations in this paper. This model has two different current equations for two different cases. For $\phi_t < \phi_B$, the mathematical representation of this model is given by

$$J_{\mathrm{GTT}} = \frac{qC_tN_t}{E}\left[\int_{\phi_B}^{\phi_t+Ed}\left(\frac{1}{P_1}+\frac{1}{P_{2\_\mathrm{trapezoid}}}\right)^{-1}d\phi\right] \quad \text{for } E_{\min} < E \leqslant \frac{\phi_B}{d}, \tag{A1}$$

$$J_{\mathrm{GTT}} = \frac{qC_tN_t}{E}\left[\int_{\phi_B}^{Ed}\left(\frac{1}{P_1}+\frac{1}{P_{2\_\mathrm{triangle}}}\right)^{-1}d\phi + \int_{Ed}^{\phi_t+Ed}\left(\frac{1}{P_1}+\frac{1}{P_{2\_\mathrm{trapezoid}}}\right)^{-1}d\phi\right] \quad \text{for } E > \frac{\phi_B}{d}. \tag{A2}$$

Note that the integration limit starts from ϕ_B and not from ϕ_t, because in this model tunneling above the metal Fermi level is not considered. $E_{\min}$ is the minimum field, below which the GTT current is zero due to the absence of traps below ϕ_B [see Fig. 2(a)], and is given by

$$E_{\min} = \frac{\phi_b - \phi_t}{d}. \tag{A3}$$

For $\phi_t > \phi_B$, the mathematical representation of this model is

$$J_{\mathrm{GTT}} = \frac{qC_tN_t}{E}\left[\int_{\phi_t}^{\phi_t+Ed}\left(\frac{1}{P_1}+\frac{1}{P_{2\_\mathrm{trapezoid}}}\right)^{-1}d\phi\right] \quad \text{for } E \leqslant \frac{\phi_t}{d}, \tag{A4}$$

$$J_{\mathrm{GTT}} = \frac{qC_tN_t}{E}\left[\int_{\phi_t}^{Ed}\left(\frac{1}{P_1}+\frac{1}{P_{2\_\mathrm{triangle}}}\right)^{-1}d\phi + \int_{Ed}^{\phi_t+Ed}\left(\frac{1}{P_1}+\frac{1}{P_{2\_\mathrm{trapezoid}}}\right)^{-1}d\phi\right] \quad \text{for } E > \frac{\phi_t}{d}. \tag{A5}$$

Since $\phi_t > \phi_B$, the integration limit starts from ϕ_t and not from ϕ_B. All the symbols in the above equations are same as in Eqs. (1)–(5).

[1] X. R. Cheng, Y. C. Cheng, and B. Y. Liu, J. Appl. Phys. **63**, 797 (1988).
[2] L. Larcher, A. Paccagnella, and G. Ghidini, IEEE Trans. Electron Devices **48**, 285 (2001).
[3] E. Suzuki and D. K. Schroder, J. Appl. Phys. **60**, 3616 (1986).
[4] S. Fleischer and P. T. Lai, J. Appl. Phys. **72**, 5711 (1992).
[5] M. P. Houng, Y. H. Wang, and W. J. Chang, J. Appl. Phys. **86**, 1488 (1999).
[6] S. Karmalkar, D. Mahaveer Sathaiya, and M. S. Shur, Appl. Phys. Lett. **82**, 3976 (2003).
[7] S. Mizuno, Y. Ohno, S. Kishimoto, K. Maezawa, and T. Mizutani, Jpn. J. Appl. Phys., Part 1 **41**, 5125 (2002).
[8] E. J. Miller, X. Z. Dang, and E. T. Yu, J. Appl. Phys. **88**, 5951 (2000).
[9] W. Quan, D. M. Kim, and M. K. Cho, J. Appl. Phys. **92**, 3724 (2002).
[10] M. S. Shur, A. D. Bykhovski, R. Gaska, and A. Khan, in *Handbook of Thin Film Devices*, edited by M. H. Francombe (Academic, San Diego,

2000), Vol. 1, p. 299.
[11]S. Karmalkar, N. Satyan, and D. M. Sathaiya, IEEE Electron Device Lett. **27**, 87 (2006).
[12]H. Hasegawa, T. Inagaki, S. Ootomo, and T. Hashizume, J. Vac. Sci. Technol. B **21**, 1844 (2003).
[13]A. van der Ziel, *Solid State Physical Electronics* (Prentice-Hall, New Delhi, India, 1971).
[14]E. H. Rhoderick and R. H. Williams, *Metal-Semiconductor Contacts* (Clarendon, Oxford, 1978).
[15]R. Hackam and P. Harrop, Solid State Commun. **11**, 669 (1972).
[16]V. Bougrov, M. Levinshtein, S. Rumyantsev, and A. Zubrilov, in *Properties of Advanced Semiconductor Materials*, edited by M. E. Levinshtein, S. L. Rumyantsev, and M. S. Shur (Wiley, New York, 2001), p. 1.
[17]E. T. Yu *et al.*, Appl. Phys. Lett. **73**, 1880 (1998).